



Research paper

Caesium incorporation and retention in illite interlayers



Adam J. Fuller ^{a,1}, Samuel Shaw ^b, Michael B. Ward ^c, Sarah J. Haigh ^{d,e}, J. Frederick W. Mosselmans ^f,
Caroline L. Peacock ^a, Stephen Stackhouse ^a, Andrew J. Dent ^f, Divyesh Trivedi ^g, Ian T. Burke ^{a,*}

^a School of Earth and Environment, University of Leeds, Leeds LS2 9JT, UK

^b School of Earth, Atmospheric and Environmental Science, University of Manchester, Manchester M13 9PL, UK

^c Leeds Electron Microscopy and Spectroscopy Centre, School of Process Environmental and Materials Engineering, University of Leeds, LS2 9JT, UK

^d SuperSTEM, STFC Daresbury Laboratories, Keckwick Lane, Warrington WA4 4AD, UK

^e School of Materials, University of Manchester, Manchester M13 9PL, UK

^f Diamond Light Source, Harwell Science and Innovation Campus, Didcot, Oxfordshire OX11 0DE, UK

^g National Nuclear Laboratory Ltd., Chadwick House, Warrington Road, Birchwood Park, Warrington WA3 6AE, UK

ARTICLE INFO

Article history:

Received 11 November 2014

Received in revised form 6 February 2015

Accepted 8 February 2015

Available online 23 February 2015

Keywords:

Cs

TEM

Illite

DFT

EXAFS

ABSTRACT

Radioactive caesium (chiefly ¹³⁷Cs) is a major environmental pollutant. The mobility of Cs in temperate soils is primarily controlled by sorption onto clay minerals, particularly the frayed edges of illite interlayers. This paper investigates the adsorption of Cs to illite at the molecular scale, over both the short and long term. Transmission electron microscopy (TEM) images showed that after initial absorption into the frayed edges, Cs migrated into the illite interlayer becoming incorporated within the mineral structure. Caesium initially exchanged with hydrated Ca at the frayed edges, causing them to collapse. This process was irreversible as Cs held in the collapsed interlayers was not exchangeable with Ca. Over the long term Cs did not remain at the edge of the illite crystals, but diffused into the interlayers by exchange with K. Results from extended X-ray absorption fine structure spectroscopy (EXAFS) and density functional theory modelling confirmed that Cs was incorporated into the illite interlayer and revealed its bonding environment.

© 2015 The Authors. Published by Elsevier B.V. This is an open access article under the CC BY license (<http://creativecommons.org/licenses/by/4.0/>).

1. Introduction

The ubiquity of ¹³⁷Cs in nuclear waste means that it is one of the most common radionuclides released into the environment by human action. Once released, the relatively long half-life ($t_{1/2}$ 30 years) and large dose rate of ¹³⁷Cs mean that it poses a potential long term radiation risk. The nuclear accidents at Chernobyl, and more recently at Fukushima, demonstrated this most acutely. In both these cases, radiocaesium remains the key contributor to radioactive dose and the reason for maintaining the exclusion zone (Jacob et al., 2009; Kinoshita et al., 2011). Additionally ¹³⁷Cs is a common contaminant at nuclear sites, such as Hanford and Sellafield, due to historic releases (Chorover et al., 2008; Reeve and Eilbeck, 2009).

Caesium is highly soluble and is present in groundwater as the monovalent Cs⁺ cation under all conditions of Eh and pH. Due to this, its concentration in solution (and thus its environmental mobility) is primarily controlled by retention on the surfaces of soil minerals, primarily through cation exchange (Sawhney, 1972; Cornell, 1993;

Hird et al., 1996). Caesium does not readily adsorb onto iron oxide minerals (Todorovic et al., 1992; Wang et al., 2000) and it is therefore principally adsorbed on clay mineral surfaces (especially in organic poor soils) (Grutter et al., 1990; Shenber and Eriksson, 1993b; Chibowski and Zygumnt, 2002). However, the sorption behaviour of Cs varies greatly between the different clay minerals and the different exchange sites on those clays. Caesium adsorption to clays occurs via several different mechanisms, including outer-sphere adsorption to planar surfaces, edge adsorption and intercalation into structural sites (Jacobs and Tamura, 1960; Hird et al., 1996; Bradbury and Baeyens, 2000). Here, and throughout this paper, outer-sphere adsorption is defined as electrostatic bonding of a hydrated ion to a surface, inner-sphere adsorption as direct bonding (electrostatic or covalent) of the dehydrated ion to the surface reactive site and absorption as incorporation into the clay structure (including within a collapsed interlayer). The dominant adsorption process within a particular environment, is dependent on a number of factors, including Cs concentration, clay structure and solution pH (Fuller et al., 2014). Multiple studies have shown that Cs is preferentially removed from solution and retained on the surfaces of soil minerals even when the total ionic-strength of other cations is very high (Brouwer et al., 1983; Dyer et al., 2000; Chorover et al., 2008). Studies from soils with varying mineralogy showed that this selective adsorption and retention of Cs was occurring primarily on illite

* Corresponding author. Tel.: +44 113 3437532.

E-mail address: i.t.burke@leeds.ac.uk (I.T. Burke).

¹ Present address: Centre for Radiochemistry Research, School of Chemistry, University of Manchester, Manchester, M13 9PL.

(K,Ca,Mg) (Al,Mg,Fe)₂ (Si,Al)₄ O₁₀ [(OH)₂,(H₂O)] (Cremers et al., 1988). The illite structure consists of 2:1 layers with two Si/Al tetrahedral sheets and a central octahedral sheet (Si/Al/Fe/Mg) which are bound together by interlayer cations. Illite commonly has K in its interlayer site which yields an overall basal spacing of 1.0 nm. However, other monovalent and divalent cations are able to exchange with the K ions and distort the structure. Most commonly illite weathers to vermiculite via the exchange of K ions for Ca (Jackson et al., 1952). As Ca is strongly hydrated it retains its waters of hydration in the interlayer causing an expansion of the illite basal spacing to 1.4 nm (Jackson et al., 1952; Jackson, 1968). This Ca weathering yields a partially expanded wedge zone between the hydrated and dehydrated interlayers, commonly called the frayed edge (Nakao et al., 2008). These frayed edge sites have been shown to selectively adsorb Cs, in preference to other monovalent and divalent cations (Chorover et al., 2008; Nakao et al., 2008). It has also been shown that once caesium is adsorbed into the frayed edge sites it cannot be readily desorbed back to solution, making these sites extremely important in controlling the long term retention of Cs in the environment, and controlling its mobility (Comans et al., 1991; de Koning and Comans, 2004). Frayed edges may also occur on other micaceous clays (McKinley et al., 2004; Wampler et al., 2012), however Cs is not as strongly held on these non-illitic frayed edges as it is in illite (Ohnuki and Kozai, 2013). Poinssot et al. (1999) and Sawhney (1966) showed that this sorption to the illite frayed edge sites was controlled by kinetics, taking more than a year to reach sorption equilibrium. To explain this Comans et al. (1991) and Comans and Hockley (1992) speculated that uptake occurs via a two stage adsorption process with both rapid cation exchange onto frayed edge sites and a much slower mechanism, potentially involving the illite interlayer spaces. Caesium is known to be able to adsorb into the interlayer of expanding clays but via different mechanisms. Specifically Cs is weakly adsorbed electrostatically in outer-sphere complexes (through interstitial waters) in the hydrated interlayer of montmorillonite (Bostick et al., 2002; Ohnuki and Kozai, 2013). It can also adsorb into the interlayer space of vermiculite, in inner-sphere complexes, potentially due to a collapse of the interlayer space, or the presence of a frayed edge (Bostick et al., 2002; Wampler et al., 2012). In addition to these interlayer sorption processes Cs is also known to adsorb via simple cation exchange onto the permanent charge sites on the clay basal plane. This process is not ion specific and is strongly controlled by solution ionic strength (Fuller et al., 2014).

Although previous authors have offered a detailed description of macro-scale Cs adsorption on illite; there is a significant gap in understanding the molecular-scale mechanisms governing these observations. However, significant advances have been made in recent years on understanding the sorption of Cs to other closely related micaceous minerals at the molecular scale. Most of this work has relied on High Resolution Transmission Electron Microscopy (HRTEM). McKinley et al. (2004) were the first to show the potential of TEM imaging to identify the site of Cs adsorption in biotite and muscovite. They showed that Cs accumulated around the edge of microscopic (many hundreds of microns across) biotite crystals. They were also able to observe inclusions of Cs deeper in the crystal, but attributed this to the presence of frayed edges at intra-particle defects. They were not able to observe any migration of Cs into the interlayer space, due to the short time period of the experiments (Comans and Hockley, 1992). More recently, work by Kogure et al. (2012), Okumura et al. (2014), and Tamura et al. (2014) has successfully shown that Cs is able to penetrate deep into the hydrated interlayer of both vermiculite and phlogopite. Specifically, Kogure et al. (2012) directly observed that Cs was incorporated into the vermiculite interlayer via exchange with hydrated Mg ions. Tamura et al. (2014) observed this same process occurring on a Mg altered phlogopite. Interestingly they noted that Cs would not readily exchange for the dehydrated K in interlayer spaces of natural (unaltered) phlogopite. They suggested that this process may be kinetically hindered (as previously suggested by Comans and Hockley (1992)) and that the equilibrium times within their experiments were not

long enough. Okumura et al. (2014) recently presented direct observation of Cs exchange for K-phlogopite interlayer spaces. They observed that Cs did not uniformly exchange all interlayers but favoured some over others. They suggested that this may be due to inhomogeneity within the clay structure, and stressed the importance of determining if this process occurred in other micaceous clays (with a different 2:1 layer structure). Therefore, although significant advances have been made in recent years in understanding Cs incorporation into mica; it remains an unanswered question whether these same processes are controlling the long term sorption and retention of Cs in illite. This is particularly important as Cs is adsorbed and retained by illite in preference to other ions (Poinssot et al., 1999; Steefel et al., 2003) and so long term Cs behaviour at many contaminated sites (such as Sellafield in the UK) is known to be controlled primarily by illite (Randall et al., 2004; Dutton et al., 2009).

This paper has two key aims. Firstly, to directly characterise the nature of the illite frayed edge and determine the mechanism of Cs adsorption therein. Secondly, to understand the migration of Cs deeper into the illite interlayer space. This work is driven by the hypothesis that the same interlayer incorporation mechanism observed in other micaceous clays occurs in illite. However, it has been shown that Cs takes a long time to reach equilibrium with the illite interlayer, likely due to stronger interlayer forces in illite than in previously studied clays. Therefore to ensure that sufficient concentrations of Cs were taken into the illite structure the experiments in this study were performed for long time periods (up to 1 year) and with a high Cs concentration (to increase the kinetic driving force, consistent with other authors (Kogure et al., 2012; Okumura et al., 2014; Tamura et al., 2014)). Previous microscopy studies have focused simply on the end point of Cs incorporation. However, this paper addresses the entire sorption process, from initial sorption on the frayed edge to its long term fate therein. This atomic-scale mechanistic understanding was achieved by utilising aberration corrected (scanning) transmission electron microscopy ((S)TEM), energy dispersive X-ray spectroscopy (EDX) and extended X-ray absorption fine structure spectroscopy (EXAFS), coupled with density functional theory (DFT) modelling.

2. Materials and methods

2.1. Materials

All the experiments described in this paper were conducted using Illite IMT-1, (Mg_{0.09} Ca_{0.06} K_{1.37}) [Al_{2.69} Fe(III)_{0.76} Fe(II)_{0.06} Mn_{tr} Mg_{0.43} Ti_{0.06}] [Si_{6.77} Al_{1.23}]O₂₀(OH)₄ (Hower and Mowatt, 1966) purchased from the Clay Minerals Society Source Clay Repository. This is a well characterised reference mineral from the Silver Hills, Montana, USA. To maximise the available surface area and create fresh unfrayed edges, the sample was finely crushed to <63 μm with a pestle and mortar and the particle size was verified by sieving. A 0.1 g subsample of the crushed illite was then weathered by suspension in a 0.1 mol L⁻¹ CaCl solution for one week, shaken daily. The remaining material was utilised without any chemical treatment.

Experiments were conducted with analytical grade reagents (or above) obtained from Fischer Scientific. Specifically, the CsCl was obtained as a dehydrated powder with 99.999% purity. The CaCl was obtained as CaCl₂·2H₂O powder with purity of >99.0%. The chemicals were used as received.

2.2. Batch sorption

Two distinct experimental systems were established, a system to test the short term adsorption/desorption of Cs on the Ca-weathered illite and a long term system to investigate the incorporation of Cs into the un-weathered K-interlayer.

To investigate the sorption of Cs onto the frayed edge sites the 0.1 g sample of the Ca-weathered illite was suspended in 1.0 mol L⁻¹ CsCl at

a solid:solution ratio of 1:50 in 10 mL polypropylene centrifuge tubes. The illite was exposed to the CsCl solution for one month and shaken daily. At the end of this period the tubes were centrifuged at 6000 g for 10 min to achieve solid-solution separation. The solution was then decanted and the illite washed 3 times with deionised water (DIW) to remove any excess salts. Half of the illite was then decanted and dried at 40 °C. The remaining material was retained to investigate Cs desorption. Desorption was performed by subjecting the Cs-illite to the same Ca weathering procedure as the natural K-illite. Specifically the illite was suspended in the 0.1 mol L⁻¹ CaCl solution for 1 week and shaken daily before being sampled as previously described.

For the long term experiments 0.1 g samples of the crushed, unweathered illite were suspended in a 1 mol L⁻¹ CsCl solution at a solid solution ratio of 1:50 in 10 mL polypropylene centrifuge tubes. The samples were then shaken weekly. Individual tubes were destructively sampled at 4, 7 and 12 months. The tubes were centrifuged at 6000 g for 10 min to achieve solid-solution separation. The solution was then decanted and for samples exposed to Cs the illite was washed in 0.1 mol L⁻¹ NaCl to remove any outer-sphere sorbed Cs on the basal plane sites and ensure only Cs specifically adsorbed into the interlayer remained. Additionally the sample was then washed 3 times with DIW to remove excess salts. The washed illite was then oven dried overnight at 40 °C before being prepared for the TEM.

2.3. (S)TEM imaging

For (S)TEM imaging a subsample of the illite was dispersed on a carbon-coated copper grid. A representative subsample was suspended in isopropyl alcohol and sonicated for around 5 min. A few drops of the suspension were then transferred onto the grid using a glass Pasteur pipette. This gave homogenous coverage of the grid with crystallites present at many different orientations. Bright field TEM imaging and spot EDX analyses of the Ca/Cs-illite system were performed using a Tecnai TF20 FEGTEM with an operating voltage of 200 keV and at room temperature (293 K). Ultra-high resolution bright and dark field STEM images and EDX maps were obtained using a FEI Titan G2 S/TEM at room temperature and with an operating voltage of 200 keV, with a beam current of 0.1 nA, a convergence angle of 18 mrad and a HAADF inner angle of 54 mrad. Illite is strongly affected by beam damage in the TEM (see SI) therefore all structural images were collected within 60 s of exposure. This rapid beam damage limited the maximum achievable magnification and resolution, and also precluded any repositioning of the samples during high resolution imaging.

2.4. TEM image and EDX analysis

The image processing for this work was performed using Gatan DigitalMicrograph. To determine the change in illite basal spacing associated with Cs interlayer incorporation, measurements were taken of the basal spacing of both dark (assumed K filled) and bright (assumed Cs filled) interlayers. These basal spacing measurements were acquired in the following manner. Cross sections were taken from the HAADF images and yielded phase contrast histograms. In these histograms peaks and troughs represented the aluminosilicate 2:1 layers and interlayer spaces of the illite structure (see example in SI Fig. S1). The peak to peak or trough to trough distance between multiple peaks/troughs was measured and from this an average peak distance was determined. The average distance between the peaks then correlates to the average basal spacing in that transect. This process was repeated many times for both regions with both dark and bright interlayers (number of measured K/Cs interlayers, *n*, shown in Fig. 2). This gave a range of values for which a mean, mode and standard deviation were determined. Difference between the average (mean and modal) basal spacing of both the K-layers and the Cs-layers was then determined. A Mann Whitney U test was also performed to determine the statistical validity of this difference.

The high concentration of the background electrolyte precluded analysis of changes in the solution chemistry (e.g. decreasing Cs concentration due to sorption). Therefore changes in chemical composition of the clays were determined directly by energy dispersive X-ray spectroscopy (EDX). The EDX data from the DIW control and Ca/Cs system was processed using INCA. For the long term system EDX maps of the different elements were analysed using Bruker ESPRIT software. Background subtracted EDX spectra for entire mapped particle were then extracted from the elemental maps. The atomic percentage of the different elements within the particle were then determined via a standardless Cliff–Lorimer analysis.

2.5. Density functional theory calculations

Density functional theory calculations were performed using the projector-augmented-wave implementation (Blöchl, 1994; Kresse and Joubert, 1999) of the VASP code (Kresse and Furthmüller, 1996a, 1996b). The illite models comprised 83 atoms, with the chemical composition: (M₃)[Al₅ Fe(III)₂ Mg][Si₁₄ Al₂]O₄₀(OH)₈, (where M = K or Cs), in order to match the sample used in the experiments as well as possible. Isomorphic substitutions in the tetrahedral sheet were placed far apart, in line with the observations of Militzer et al. (2011). Changing the arrangement of isomorphic substitution caused variations in basal spacing of about 0.01 Å.

The models were optimized with a kinetic energy cut-off for the plane-wave expansion of 800 eV and Brillouin-zone sampling restricted to the Γ -point. These settings ensured that calculated basal spacings were converged to within about 0.01 Å. The potentials were generated using the electronic configurations: 2p⁶3s² for magnesium, 3d⁷4s¹ for iron, 5s²5p⁶6s¹ for caesium, 3s²3p¹ for aluminium, 1s¹ for hydrogen, 3s²3p² for silicon, and 2s²2p⁴ for oxygen. The calculations were spin polarised with iron modelled in a high-spin state. All calculations were performed using both the local density approximation (LDA) (Perdew and Zunger, 1981) and PBE formulation of the generalised gradient approximation (GGA) (Perdew et al., 1996).

2.6. EXAFS

Cs K-edge (35,985 keV) spectra were gathered on beamline B18 at the Diamond Light Source, Didcot, UK. During data collection the sample was held in an Oxford Instruments cryostat at 80 K to enhance data quality and reduce the chance of radiation damage. Cs K-edge spectra were then gathered in fluorescence mode using a 9 element Ge solid state detector. To improve the signal to noise ratio a total of 144 5-minute scans were gathered and averaged using Athena (Ravel and Newville, 2005). The default background subtraction provided by Athena was accepted and this final data was used for fitting.

The EXAFS data was analysed using Artemis (Ravel and Newville, 2005) running Feff6.0 (Rehr and Albers, 2000). The initial model used was constructed using data from the density functional theory (DFT) calculations.

3. Results and discussion

3.1. Formation of and Cs absorption into the frayed edge sites

Initially a series of experiments were performed to investigate the formation of the frayed edge sites and the absorption of Cs therein. Fig. 1 shows bright field TEM micrographs of the illite material (a) prior to any chemical treatment (b) after suspension in 1 mol L⁻¹ CaCl (c) after suspension of the CaCl weathered illite in 1 mol L⁻¹ CsCl and finally (d) after suspension of the Cs-illite in CaCl. In the original material all the imaged crystals were found to have a constant 1.0 nm basal spacing (i.e. 2:1 layer + interlayer space) along their full length (Fig. 1a) confirming that the material was unweathered and no frayed edge sites were present. This structure remained stable when immersed

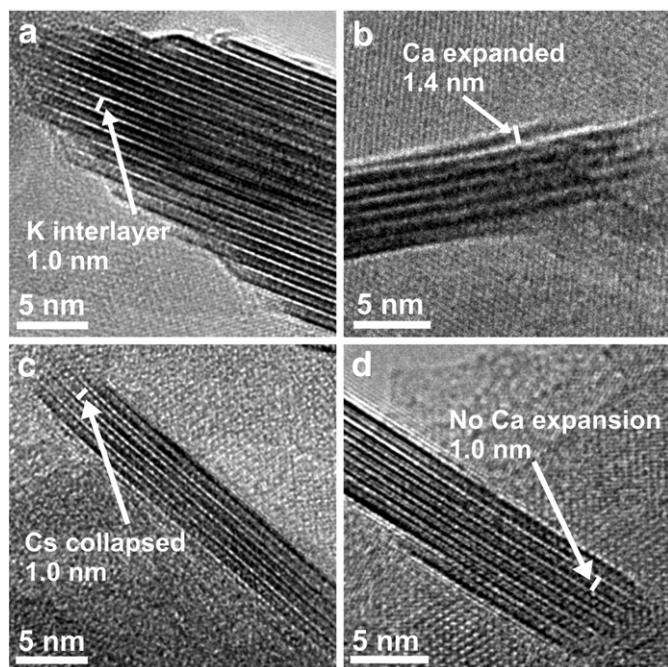


Fig. 1. Expansion and collapse of the illite interlayer. (a) The initial illite material shows a stable 1.0 nm basal spacing. (b) The edges of the illite expand to 1.4 nm upon sorption of Ca. (c) Exchange of the edge sorbed Ca for Cs causes a dehydration and re-collapse of the interlayer (d) Cs held in this collapsed interlayer was not exchanged by Ca and the structure did not re-expand.

in deionised water for 4 months and there was no detectable reduction in K concentration (SI section S2 and Figs. S2 and S3). However, when the illite was suspended in CaCl the edges of the crystals expanded, giving a basal spacing of 1.4 nm (Fig. 1b). EDX confirmed that there was Ca present in these expanded edge regions and that they were deficient in K, relative to the original material (SI Fig. S4b). This frayed edge region extended up to 5 nm into the interlayer. Fig. 1a and b shows the well documented mechanism of illite weathering which liberates the interlayer K ions (Jackson and Doring, 1979; Sparks and Huang, 1985; Moritsuka et al., 2004) and causes the formation of the frayed edge sites. The 1.4 nm spacing is only possible if the Ca remains in hydrated outer-sphere complexes, where it is easily exchanged (Comans et al., 1991; Nakao et al., 2008). Therefore the frayed edges are more hydrated than the stable K-illite interlayers.

Once the illite had been successfully weathered with Ca and 'frayed edges' formed it was possible to investigate the absorption of Cs into the 'frayed edge'. Fig. 1c shows that after suspension of the Ca-illite in Cs for one month the edges had recollapsed from 1.4 nm to 1.0 nm. After this treatment no Ca was detected in the edges by EDX (SI Fig. S4c). Instead, a small concentration of Cs was detected in the structure. Therefore it can be asserted that the Cs was absorbed into the frayed edge site via cation exchange with the Ca ions. This exchange caused the edges to collapse back down to 1.0 nm. This likely occurred due to dehydration of the interlayer space as Cs is less strongly hydrated than Ca (Rosso et al., 2001). This mechanism of expansion and collapse has been proposed for many decades in both the radiochemistry and mineral weathering literature (Jackson et al., 1952; Sawhney, 1967; Benedicto et al., 2014). In this current work this process is observed to be occurring with Cs in illite. To investigate the reversibility of this Cs absorption, the samples were resuspended in a Ca solution to attempt to re-expand the Cs-interlayers with Ca. However this appeared to be unsuccessful. No Ca sorption was detected in EDX chemical analysis (SI Fig. S4d) and Fig. 1d shows that the structure remained unexpanded at 1.0 nm. This unexpandable nature of the Cs-interlayer was proposed by de Koning and Comans (2004) as a likely explanation for irreversibility of Cs absorption into illite. This lack of Cs desorption from illite has been widely

observed (Shenber and Eriksson, 1993a; Bellenger and Staunton, 2008; Gil-García et al., 2008) and attributed to specific retention in the frayed edges (Willms et al., 2004). The new results presented here confirmed this lack of re-expansion of the collapsed frayed edges and offer an explanation for the irreversibility of Cs absorption, even after short contact periods, consistent with de Koning and Comans (2004).

3.2. Long term Cs interlayer incorporation

Beyond the short term absorption of Cs to expanded Ca-interlayers it is important to understand the long term fate of Cs in the collapsed K-interlayer region. Cs absorption can take over a year to reach equilibrium (Sawhney, 1966; Comans et al., 1991; Comans and Hockley, 1992; Konoplev et al., 1996; Poinssot et al., 1999) so it was crucial to study the progress of illite incorporation over this timescale. Fig. 2 presents High Angle Annular Dark Field (HAADF) STEM micrographs of illite viewed along the clay layers at different stages during the process of Cs absorption. Assuming uniform thickness, the intensity of the HAADF image is proportional to the square of the mean atomic number; allowing layers with different compositions within the clay structure to be identified. Specifically in the natural illite starting material (Fig. 2a) EDX analysis (SI Fig. S5a) confirmed that the structure consisted dominantly of Si ($Z = 14$), Al ($Z = 13$) and O ($Z = 8$) atoms in the 2:1 layers and K ($Z = 19$) in the interlayer. However, the 2:1 layers appear brighter than the interlayer due to significant Fe ($Z = 26$) substitution in the octahedral sheet. In contrast, HAADF images of the samples exposed to Cs for 4 or 7 months showed interlayer spaces that varied in intensity, even within a single crystal (Fig. 2b and c). In these samples a number of the interlayers were brighter than the 2:1 layers (Fig. 2b). Additionally in some of the illite crystallites a single interlayer was partially brighter than the 2:1 layer and partially darker (Fig. 2c). The brightness in these interlayers indicates that the mean atomic number (Z) is greater than either the 2:1 layers or the darker interlayers. Caesium ($Z = 55$) will give higher intensity than either K ($Z = 19$) or the Fe ($Z = 26$) in the 2:1 layers in a HAADF image, suggesting that these bright interlayers contain Cs. The presence of Cs in both of these samples was also confirmed by EDX (SI Fig. S5b). This phenomenon of heterogeneous interlayer filling was also observed by Okumura et al. (2014) for Cs incorporation into phlogopite. The reason for this heterogeneous distribution of Cs between interlayers is unclear but may be due to variation in layer charge on the aluminosilicate 2:1 layers leading to a difference in Cs/K exchange rates. Once exchange has begun the interlayer provides a fast diffusion path, meaning it is then possible for the Cs ions to diffuse into and exchange the whole interlayer space to attain the energetically more favourable Cs substituted structure (Rosso et al., 2001). Alternatively, Cs may be absorbed into vacant interlayer sites (rather than exchanged with K) that are present in these interlayer spaces, but not in others. By 12 months the majority of the interlayers in the imaged sample appear to be bright, consistent with them being Cs filled (Fig. 2d). An EDX analysis of the 12 month sample also showed significant concentrations of Cs in the structure (SI Fig. S5d and Table S1).

In addition to the phase contrast and EDX evidence for the incorporation of Cs into the interlayer space the effect of changing interlayer cation on the mineral structure was also examined. To determine this change, a large number of unit layers (2:1 layer and interlayer space), with both dark ($n = 180$) and bright ($n = 31$) interlayers, were measured. Fig. 2e shows the range and frequency of measured basal spacings. From these results it was determined that the basal spacing of those regions with brighter interlayers was on average 0.07 nm larger than the less bright interlayers (Fig. 2e), showing a significant expansion (Mann Whitney U; $p < 0.001$). Density functional theory modelling was then used to determine if these basal spacings, and the associated change, were caused by the exchange of K for Cs in the interlayer site. A density function theory model was constructed with either K or Cs in the interlayer site. The modelling was performed using both the local density approximation (LDA) and the generalised gradient

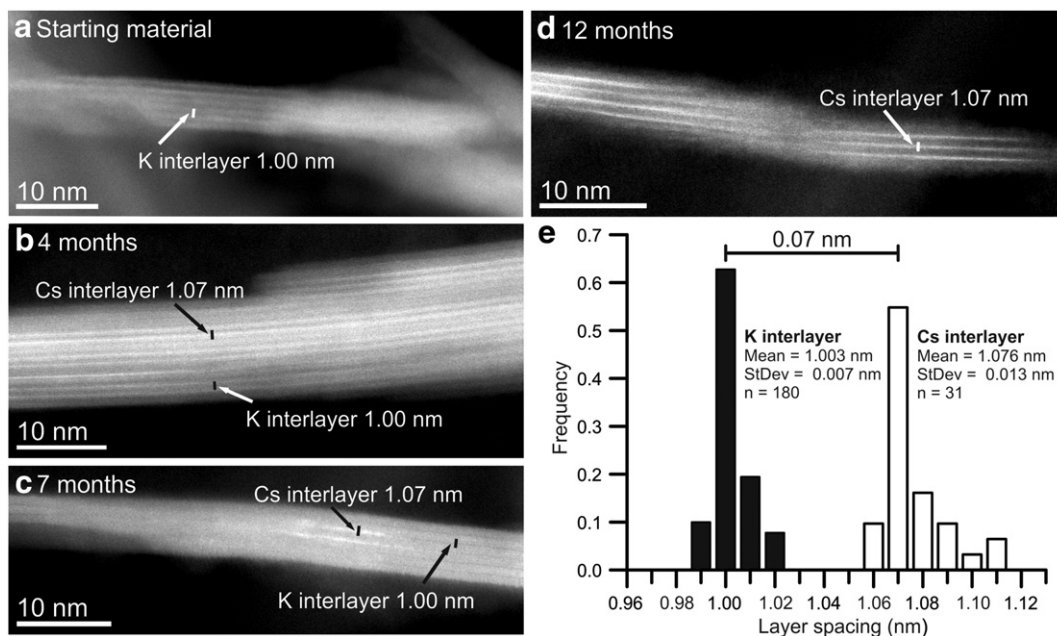


Fig. 2. HAADF images of Cs interlayer incorporation. (a) Starting illite shows planes with uniform brightness and a constant basal spacing of 1.00 nm suggesting that the material has a constant composition throughout the structure. (b) After 4 months and (c) 7 months Cs exposure some of the illite interlayer spaces are brighter than others, indicating local interlayer regions with a higher atomic number. (d) In illite exposed to Cs for 12 months all of the interlayers are again of uniform intensity but now with an expanded basal spacing of 1.07 nm suggesting that all interlayers are Cs filled. (e) The basal spacing measured from the dark K interlayers (black bars) and bright Cs interlayers (white bars) n , number of measured interlayers across all samples (used to determine means).

approximation (GGA). The resulting lattice parameters are shown in the SI (Table S2). The basal spacings predicted using the LDA and GGA differ by about 0.05 nm. This is in accordance with the well-known fact that the LDA underestimates lattice parameters, while the GGA overestimates them. The average measured basal spacing for the K- and Cs-illite from the experimental samples was between the two model predictions. Specifically for the K-illite the LDA model gave a basal spacing of 0.97 nm, GGA gave 1.03 nm and the measured result was on average 1.00 nm. For Cs-illite, LDA gave 1.04 nm and GGA gave 1.09 nm where

the average measured spacing was 1.08 nm. Additionally, close agreement was found between the modelled changes in basal spacing, when going from K to Cs, being 0.064 nm with the LDA approximation and 0.071 nm for GGA. This was also consistent with the measured change in basal spacing of 0.07 nm. Therefore, density functional theory modelling and direct measurements strongly support the conclusion that the bright interlayer spaces in the HAADF images are due to Cs absorption into the illite structure. This change in layer-spacing has been previously proposed to occur when Cs incorporates into aluminosilicates (Kogure

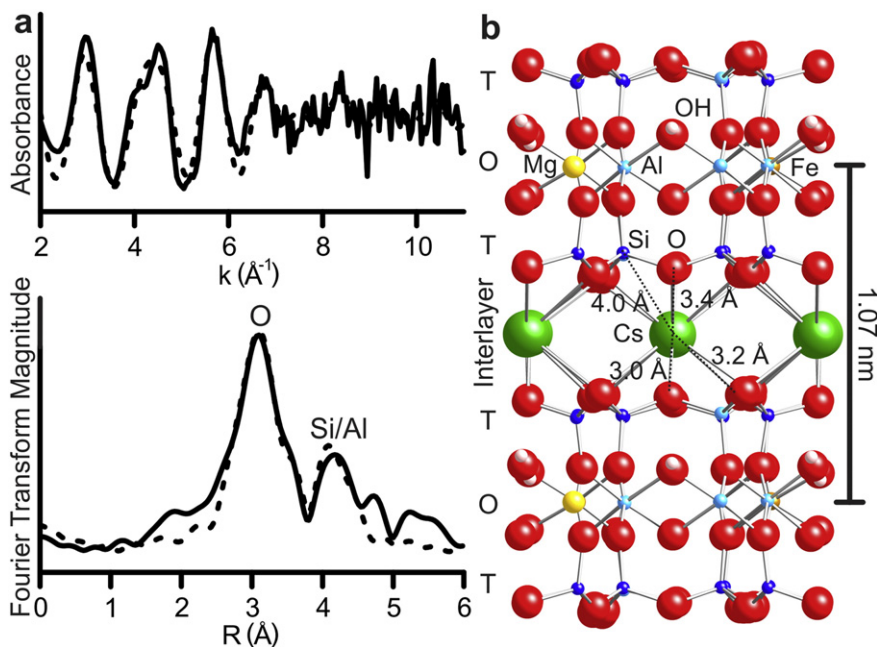


Fig. 3. Structural coordination of Cs in the illite interlayer (a) k -space EXAFS spectra and Fourier transform of the EXAFS (solid line) with the refined fit (dotted lines) for 12 oxygen atoms at 3.0–3.3 Å and 12 silicon atoms at 4.0 Å. (b) Crystallographic model of the Cs substituted illite determined by DFT calculations. Atoms and interatomic distances used to fit the EXAFS data are annotated.

et al., 2012; Tamura et al., 2014), further supporting the validity of the measurements presented here.

Extended X-ray absorption fine structure spectroscopy (EXAFS) was used to determine the nature of the bonding environment for Cs incorporated into the illite interlayer space. Fig. 3a shows the EXAFS data and calculated fit (dotted line). The fit to the EXAFS data was based on the Cs local environment determined from DFT calculations for Cs-filled illite, shown in Fig. 3b (SI Table S2). From the DFT it was determined that the Cs should be coordinated by 12 oxygen atoms at 3.0–3.4 Å and 12 silicon atoms at 4.0 Å (coordinating atoms and interatomic distances shown in Fig. 3b). For the EXAFS fit similar length paths were grouped together, such that the initial model of O neighbours used was 2 at 3.04 Å, 4 at 3.12 Å and 6 at 3.40 Å with 12 Si atoms at 3.94 Å (Table 1). Differentiating between Si and Al in EXAFS is difficult; hence this last shell accounts for the signal due to both Si and Al scatterers. The inter-atomic distance and Debye–Waller factor for each shell, E_0 and S_0^2 were refined in R-space using a range of 1.9–3.9 Å in R-space, keeping the number of atoms in each shell constant. To reduce the number of variables the Debye–Waller factors for the first two O shells were fixed to be the same value. The fit was made to the k , k^2 and k^3 -weighted Fourier transforms using a range 2.5–11 Å⁻¹ in k -space simultaneously. Once the best fit had been achieved each shell was removed in turn to check its significance. No reasonable fit could be achieved with only 3 shells of atoms. The Debye–Waller factors for the third O shell and the Si–Al shell are somewhat large, because they represent the average of individual scattering paths covering a wide spread of distances (ca 0.25 and 0.14 Å respectively).

This refined EXAFS fit yielded parameters which matched the distances and coordination numbers determined by the DFT model (within error) (Table 1). Therefore it can be asserted that after 12 months, ~90% of the Cs in the sample is present in the illite interlayer, consistent with the HAADF STEM imaging. Previous EXAFS studies of Cs adsorption to various clays offered quite different spectra and coordination environments for Cs, as they failed to get interlayer incorporation (Bostick et al., 2002) or had a signal dominated by outer-sphere complexes (Nakano et al., 2003; Fan et al., 2014). The high loadings and long exposure times used in this study yielded a high enough concentration of Cs in the interlayer space to fully resolve its coordination environment, when held in inner-sphere complexes.

Table 1

Artemis model fitting parameters for Cs K-edge EXAFS: n, site occupancy; r, inter-atomic bond distance; σ^2 , Debye–Waller factor. Reduced Chi squared for this fit = 116, R-Factor = 0.020 $S_0^2 = 1.05$, $E_0 = 6.4$ eV.

Shell	n	r (Å)	σ^2
O	2	3.00 (± 0.03)	0.0062 (± 0.04)
O	4	3.16 (± 0.02)	0.0062 (± 0.04)
O	6	3.34 (± 0.03)	0.0131 (± 0.04)
Si/Al	12	3.99 (± 0.03)	0.0320 (± 0.04)

EDX maps were gathered to further confirm that Cs was incorporated into the illite structure, rather than being sorbed to the basal plane. Fig. 4 shows a HAADF image and accompanying EDX maps looking down onto two illite crystals (i.e. perpendicular to the layers). The maps clearly show that both Cs and K are homogeneously distributed throughout the crystals at the length scale imaged. There is no evidence for any enhancement in Cs concentration at the edge, with Cs detected up to ~100 nm from the edge of the crystal. In EDX maps signal intensity is related to atomic abundance and sample thickness (Fitting et al., 1977). Normalisation of the EDX spectra from the two crystals shown reveals that they have an identical Cs/K ratio (Fig. 4f). Therefore, the difference in HAADF intensity observed is ascribed to thickness effects. The Cs signal varies with thickness proportionally to the other elements (SI Fig. S6) suggesting that the Cs must be within the interlayer space, as Cs present solely on the surface would have an EDX intensity unrelated to crystal thickness.

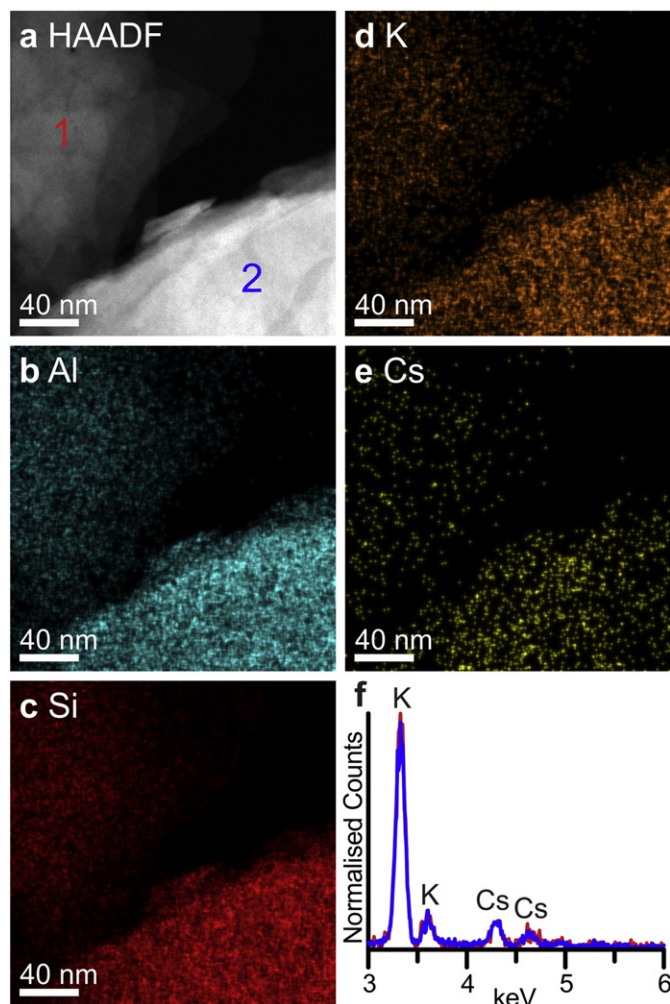


Fig. 4. EDX maps of the 12 month sample. a, HAADF image of planar surface of one thicker (brighter) and one thinner (darker) illite crystal. b, EDX map of the Al signal, stronger signal from the lower crystal is due to its greater thickness. c, Si EDX map. d, K EDX map. e, Cs EDX map. f, Normalised (on Si) EDX spectra from the two labelled crystals showing the presence of both K and Cs in the structure (full spectra SI Fig. S5).

4. Conclusions

Overall, it has been shown that Cs can initially adsorb to and become irreversibly trapped in illite interlayers due to collapse of the frayed edge sites. Therefore it can be robustly concluded that Cs held in these specific frayed edge sites will not be bio-available or mobile (in solution) in contaminated environments. Over the longer term Cs was observed to diffuse from the edges into the interior interlayer space. Although the experiments in this study were conducted at artificially high concentrations (to accelerate the kinetics) it is possible that these same mechanisms may operate at environmental levels, but over a much longer time period. This would explain the continuing long-term increases in Cs uptake to illite observed in previous experiments (Comans and Hockley, 1992). Therefore this interlayer incorporation is the likely long term sink for Cs in contaminated soils. Additionally, as Cs cannot be easily remobilised from this interlayer space, any effective remediation measures must either separate or degrade the illite clay fraction. This must be accounted for when considering any potential strategies for management and potential remediation of sites contaminated with radiocaesium.

Acknowledgements

This work was primarily funded by the UK Engineering and Physical Sciences Research Council (EPSRC) industrial CASE Studentship

#10000173 in partnership with National Nuclear Laboratory awarded to AJF. ChemiSTEM imaging was funded by the ESPRC SuperSTEM committee proposal #0044. SJH thanks the Defense Threat Reduction Agency (USA) under grant number HDTRA-1-12-0013. Cs K-edge EXAFS were gathered on beamline B18 at the Diamond Light Source under Rapid Access Proposal SP4901.

Appendix A. Supplementary data

Supplementary data to this article can be found online at <http://dx.doi.org/10.1016/j.clay.2015.02.008>.

References

- Bellenger, J.P., Staunton, S., 2008. Adsorption and desorption of Sr-85 and (Cs)-C-137 on reference minerals, with and without inorganic and organic surface coatings. *J. Environ. Radioact.* 99, 831–840.
- Benedicto, A., Missana, T., Fernández, A.M., 2014. Interlayer collapse affects on cesium adsorption onto illite. *Environ. Sci. Technol.* 48, 4909–4915.
- Blöchl, P.E., 1994. Projector augmented-wave method. *Phys. Rev. B* 50, 17963–17979.
- Bostick, B.C., Vairavamurthy, M.A., Karthikeyan, K.G., Chorover, J., 2002. Cesium adsorption on clay minerals: an EXAFS spectroscopic investigation. *Environ. Sci. Technol.* 36, 2670–2676.
- Bradbury, M.H., Baeyens, B., 2000. A generalised sorption model for the concentration dependent uptake of caesium by argillaceous rocks. *J. Contam. Hydrol.* 42, 141–163.
- Brouwer, E., Baeyens, B., Maes, A., Cremers, A., 1983. Cesium and rubidium ion equilibrium in illite clay. *J. Phys. Chem.* 87, 1213–1219.
- Chibowski, S., Zygmunt, J., 2002. The influence of the sorptive properties of organic soils on the migration rate of Cs-137. *J. Environ. Radioact.* 61, 213–223.
- Chorover, J., Choi, S., Rotenberg, P., Serne, R.J., Rivera, N., Strepka, C., Thompson, A., Mueller, K.T., O'Day, P.A., 2008. Silicon control of strontium and cesium partitioning in hydroxide-weathered sediments. *Geochim. Cosmochim. Acta* 72, 2024–2047.
- Comans, R.N.J., Hockley, D.E., 1992. Kinetics of cesium sorption on illite. *Geochim. Cosmochim. Acta* 56, 1157–1164.
- Comans, R.N.J., Haller, M., Depreter, P., 1991. Sorption of cesium on illite: nonequilibrium behaviour and reversibility. *Geochim. Cosmochim. Acta* 55, 433–440.
- Cornell, R., 1993. Adsorption of cesium on minerals: a review. *J. Radioanal. Nucl. Chem.* 171, 483–500.
- Cremers, A., Elsen, A., Depreter, P., Maes, A., 1988. Quantitative analysis of radiocaesium retention in soils. *Nature* 335, 247–249.
- de Koning, A., Comans, R.N.J., 2004. Reversibility of radiocaesium sorption on illite. *Geochim. Cosmochim. Acta* 68, 2815–2823.
- Dutton, M.V., Foster, C., Trivedi, D., 2009. Characterisation of Soils From B38 Site Investigation Within the Sellafield Separation Area. NNL Commercial.
- Dyer, A., Chow, J.K.K., Umar, I.M., 2000. The uptake of caesium and strontium radioisotopes onto clays. *J. Mater. Chem.* 10, 2734–2740.
- Fan, Q.H., Tanaka, M., Tanaka, K., Sakaguchi, A., Takahashi, Y., 2014. An EXAFS study on the effects of natural organic matter and the expandability of clay minerals on cesium adsorption and mobility. *Geochim. Cosmochim. Acta* 135, 49–65.
- Fitting, H.J., Glaefke, H., Wild, W., 1977. Electron penetration and energy transfer in solid targets. *Phys. Status Solidi A* 43, 185–190.
- Fuller, A.J., Shaw, S., Peacock, C.L., Trivedi, D., Small, J.S., Abrahamsen, L.G., Burke, I.T., 2014. Ionic strength and pH dependent multi-site sorption of Cs onto a micaceous aquifer sediment. *Appl. Geochem.* 40, 32–42.
- Gil-García, C.J., Rigol, A., Rauret, G., Vidal, M., 2008. Radionuclide sorption–desorption pattern in soils from Spain. *Appl. Radiat. Isot.* 66, 126–138.
- Grutter, A., Vongunten, H.R., Kohler, M., Rossler, E., 1990. Sorption, desorption and exchange of cesium on glacioluvial deposits. *Radiochim. Acta* 50, 177–184.
- Hird, A.B., Rimmer, D.L., Livens, F.R., 1996. Factors affecting the sorption and fixation of caesium in acid organic soil. *Eur. J. Soil Sci.* 47, 97–104.
- Hower, J., Mowatt, T.C., 1966. The mineralogy of illites and mixed-layerillite/montmorillonites. *Am. Mineral.* 51, 825–854.
- Jackson, M.L., 1968. Weathering of Primary and Secondary Minerals in Soils. 9th International Congress of Soil Science. The International Society of Soil Science and Angus & Robertson Ltd, Adelaide, Australia, pp. 281–292.
- Jackson, B.L.J., Doring, C., 1979. Studies of slowly available potassium in soils of New Zealand – I. Effects of leaching, temperature and potassium depletion on the equilibrium concentration of potassium in solution. *Plant Soil* 51, 197–204.
- Jackson, M.L., Hseung, Y., Corey, R.B., Evans, E.J., Heuvel, R.C.V., 1952. Weathering sequence of clay-size minerals in soils and sediments: II. Chemical weathering of layer silicates. *Soil Sci. Soc. Am. Proc.* 16, 3–6.
- Jacob, P., Fesenko, S., Bogdevitch, I., Kashparov, V., Sanzharova, N., Grebenshikova, N., Isamov, N., Lazarev, N., Panov, A., Ulanovsky, A., Zhuchenko, Y., Zhurba, M., 2009. Rural areas affected by the Chernobyl accident: radiation exposure and remediation strategies. *Sci. Total Environ.* 408, 14–25.
- Jacobs, D.G., Tamura, T., 1960. The mechanism of ion fixation using radio-isotope techniques. 7th International Congress of Soil Science. The International Society of Soil Science, Madison, Wisconsin, USA, pp. 206–214.
- Kinoshita, N., Sueki, K., Sasa, K., Kitagawa, J.-i., Ikarashi, S., Nishimura, T., Wong, Y.-S., Satou, Y., Handa, K., Takahashi, T., Sato, M., Yamagata, T., 2011. Assessment of individual radionuclide distributions from the Fukushima nuclear accident covering central-east Japan. *Proc. Natl. Acad. Sci. U. S. A.* 108, 19526–19529.
- Kogure, T., Morimoto, K., Tamura, K., Sato, H., Yamagishi, A., 2012. XRD and HRTEM evidence for fixation of cesium ions in vermiculite clay. *Chem. Lett.* 41, 380–382.
- Konoplev, A.V., Bulgakov, A.A., Popov, V.E., Hilton, J., Comans, R.N.J., 1996. Long-term investigation of Cs-137 fixation by soils. *Radiat. Prot. Dosim.* 64, 15–18.
- Kresse, G., Furthmüller, J., 1996a. Efficiency of ab-initio total energy calculations for metals and semiconductors using a plane-wave basis set. *Comput. Mater. Sci.* 6, 15–50.
- Kresse, G., Furthmüller, J., 1996b. Efficient iterative schemes for ab initio total-energy calculations using a plane-wave basis set. *Phys. Rev. B* 54, 11169–11186.
- Kresse, G., Joubert, D., 1999. From ultrasoft pseudopotentials to the projector augmented-wave method. *Phys. Rev. B* 59, 1758–1775.
- McKinley, J.P., Zachara, J.M., Heald, S.M., Dohnalkova, A., Newville, M.G., Sutton, S.R., 2004. Microscale distribution of cesium sorbed to biotite and muscovite. *Environ. Sci. Technol.* 38, 1017–1023.
- Militzer, B., Wenk, H.R., Stackhouse, S., Stixrude, L., 2011. First-principles calculation of the elastic moduli of sheet silicates and their application to shale anisotropy. *Am. Mineral.* 96, 125–137.
- Moritsuka, N., Yanai, J., Kosaki, T., 2004. Possible processes releasing nonexchangeable potassium from the rhizosphere of maize. *Plant Soil* 258, 261–268.
- Nakano, M., Kawamura, K., Ichikawa, Y., 2003. Local structural information of Cs in smectite hydrates by means of an EXAFS study and molecular dynamics simulations. *Appl. Clay Sci.* 23, 15–23.
- Nakao, A., Thiry, Y., Funakawa, S., Kosaki, T., 2008. Characterization of the frayed edge site of micaceous minerals in soil clays influenced by different pedogenetic conditions in Japan and northern Thailand. *Soil Sci. Plant Nutr.* 54, 479–489.
- Ohnuki, T., Kozai, N., 2013. Adsorption behavior of radioactive cesium by non-mica minerals. *J. Nucl. Sci. Technol.* 50, 369–375.
- Okumura, T., Tamura, K., Fujii, E., Yamada, H., Kogure, T., 2014. Direct observation of cesium at the interlayer region in phlogopite mica. *Microscopy* 63, 65–72.
- Perdew, J.P., Zunger, A., 1981. Self-interaction correction to density-functional approximations for many electron systems. *Phys. Rev. A* 23.
- Perdew, J.P., Burke, K., Ernzerhof, M., 1996. Generalized gradient approximation made simple. *Phys. Rev. Lett.* 77, 3865–3868.
- Poinssot, C., Baeyens, B., Bradbury, M.H., 1999. Experimental and modelling studies of caesium sorption on illite. *Geochim. Cosmochim. Acta* 63, 3217–3227.
- Randall, M.G., Brydrie, J., Graham, J., Small, J.S., 2004. SCLS Phase 1: the Geochemistry of the Sellafield Site. BNFL Commercial.
- Ravel, B., Newville, M., 2005. ATHENA, ARTEMIS, HEPHAESTUS: data analysis for X-ray absorption spectroscopy using IFEFFIT. *J. Synchrotron Radiat.* 12, 537–541.
- Reeve, P., Eilbeck, K., 2009. Contaminated land and groundwater management at Sellafield, a large operational site with significant legacy and contaminated land challenges. 11th International Conference on Environmental Remediation and Radioactive Waste Management, IREM'07, September 2, 2007 – September 6, 2007, PART A American Society of Mechanical Engineers, Bruges, Belgium, pp. 431–437.
- Rehr, J.J., Albers, R.C., 2000. Theoretical approaches to X-ray absorption fine structure. *Rev. Mod. Phys.* 72, 621–654.
- Rosso, K.M., Rustad, J.R., Bylaska, E.J., 2001. The Cs/K exchange in muscovite interlayers: an AB initio treatment. *Clays Clay Minerals* 49, 500–513.
- Sawhney, B.L., 1966. Unusual sorption on caesium by vermiculite. *Nature* 211, 893–894.
- Sawhney, B.L., 1967. Cesium sorption in relation to lattice spacing and cation exchange capacity of biotite. *Soil Sci. Soc. Am. Proc.* 31, 181–183.
- Sawhney, B.L., 1972. Selective sorption and fixation of cations by clay-minerals – review. *Clays Clay Minerals* 20, 93–100.
- Shenber, M.A., Eriksson, A., 1993a. Exchangeability of cesium in various soils. *Sci. Total Environ.* 138, 271–279.
- Shenber, M.A., Eriksson, A., 1993b. Sorption behavior of cesium in various soils. *J. Environ. Radioact.* 19, 41–51.
- Sparks, D.L., Huang, P.M., 1985. Physical chemistry of soil potassium. In: Munson, R.D. (Ed.), Potassium in Agriculture. American Society of Agronomy, Madison, pp. 201–276.
- Steefel, C.L., Carroll, S., Zhao, P., Roberts, S., 2003. Cesium migration in Hanford sediment: a multirate cation exchange model based on laboratory transport experiments. *J. Contam. Hydrol.* 67, 219–246.
- Tamura, K., Kogure, T., Watanabe, Y., Nagai, C., Yamada, H., 2014. Uptake of cesium and strontium ions by artificially altered phlogopite. *Environ. Sci. Technol.* 48, 5808–5815.
- Todorovic, M., Milonjic, S.K., Comor, J.J., Gal, I.J., 1992. Adsorption of radioactive ions $^{137}\text{Cs} + ^{85}\text{Sr}^{2+}$, and $^{80}\text{Co}^{2+}$ on natural magnetite and hematite. *Sep. Sci. Technol.* 27, 671–679.
- Wampler, J.M., Krogstad, E.J., Elliott, W.C., Kahn, B., Kaplan, D.I., 2012. Long-term selective retention of natural Cs and Rb by highly weathered coastal plain soils. *Environ. Sci. Technol.* 46, 3837–3843.
- Wang, X., Dong, W., Li, Z., Du, J., Tao, Z., 2000. Sorption and desorption of radiocesium on red earth and its solid components: relative contribution and hysteresis. *Appl. Radiat. Isot.* 52, 813–819.
- Willms, C., Li, Z.H., Allen, L., Evans, C.V., 2004. Desorption of cesium from kaolinite and illite using alkylammonium salts. *Appl. Clay Sci.* 25, 125–133.